Available online at www.sciencedirect.com
SCIENCE DIRECT®
Journal of Photochemistry and Photobiology A: Chemistry 163 (2004) 395–401
Journal of Photochemistry and Photobiology A:Chemistry
www.elsevier.com/locate/jphotochem

The effect of calcination on photocatalytic activity of TiO_2 particles: femtosecond study

Miia Salmi [a,*], Nikolai Tkachenko [a], Visa Vehmanen [b], Ralf-Johan Lamminmäki [b], Saila Karvinen [b], Helge Lemmetyinen [a]

[a] *Institute of Materials Chemistry, Tampere University of Technology, P.O. Box 541, FIN-33101 Tampere, Finland*
[b] *Kemira Pigments Oy, FIN-28840 Pori, Finland*

Received 1 December 2003; received in revised form 1 December 2003; accepted 19 January 2004

Abstract

The transient absorption properties of TiO_2 nanocrystalline anatase powder samples calcinated at different temperatures were studied by femtosecond diffuse reflectance spectroscopy. The measurements were performed in TiO_2 aqueous suspensions in the presence and absence of thiocyanate ions, SCN^-. Transient absorption decay behaviour of the TiO_2 particles was independent of calcination temperature. Both the shapes of the transient absorption spectra and the decay kinetics were practically the same for all the samples. The multiexponential global fitting analysis applied to the transient absorption data of the TiO_2/SCN^- system revealed the spectra and the lifetimes of the transient species. After the hole transfer from TiO_2 to SCN^- the consecutive formation of a weekly coupled dimeric thiocyanate radical anion, $(SCN\cdots SCN)^{\bullet -}$, and its structural stabilization to $(SCN)_2^{\bullet -}$ were observed with time constants of a few picoseconds and few tens to hundreds of picoseconds, respectively. The time constants were dependent on the calcination temperature of the TiO_2 particles being the faster the lower was the calcination temperature. Also the relative amounts of the formed $(SCN\cdots SCN)^{\bullet -}$ and $(SCN)_2^{\bullet -}$ were dependent on the calcination temperature of the TiO_2 samples. The extent of the initial fast hole transfer reaction correlated with the calcination temperature being the more intensive the lower was the calcination temperature. On the other hand, relatively more $(SCN)_2^{\bullet -}$ were formed at longer timescales the higher was the calcination temperature.

Keywords: TiO_2; Photocatalysis; Femtosecond diffuse reflectance spectroscopy; Calcination

1. Introduction

TiO_2 is one of the most promising semiconductor photocatalysts and a lot of research has been done concerning its applications toward solar energy conversion and environmental cleanup [1–8]. Charge carrier dynamics on the surface of a metal oxide based catalyst plays a key role in photochemical processes. Lifetimes of photogenerated charge carriers on TiO_2 and rates of the charge transfer processes between TiO_2 and a molecule adsorbed on its surface are considered to be important factors affecting the efficiency of heterogenous photochemical reactions.

The time-resolved absorption spectroscopy has been used for investigation of the dynamics of the charge carriers [1,7]. Recently time-resolved pump-probe spectroscopy measurements have revealed the kinetics of the charge carrier trapping, recombination, and charge transfer processes in femtosecond and picosecond time-ranges. First measurements were performed in colloidal TiO_2 solutions using transmittance-mode optical alignment [9–12]. Femtosecond diffuse reflectance spectroscopy, in which diffuse reflected light from the sample is used as a probe light, has been applied to study the charge carrier dynamics of the TiO_2 powder systems [13–20].

Photocatalytic oxidation of the thiocyanate ion, SCN^-, by photoexcited TiO_2 is one of the systems involving the charge transfer process. The final reaction product of the SCN^- oxidation is a dimeric thiocyanate radical anion, $(SCN)_2^{\bullet -}$, which has a characteristic absorption band around 480 nm [22,23]. The flash photolysis spectroscopy [21,24–26] and recently the femtosecond pump-probe spectroscopy [12,14,18] have been applied to study the TiO_2/SCN^- systems, both in colloidal [12,21,25–26] and particulate systems [14,18,24]. Furube et al. [18] have reported results on the femtosecond diffuse reflectance spectroscopy of an interfacial hole transfer dynamics from the

* Corresponding author. Tel.: +358-3-3115-2631; fax: +358-3-3115-2108.
E-mail address: miia.salmi@tut.fi (M. Salmi).

1010-6030/$ – see front matter © 2004 Elsevier B.V. All rights reserved.
doi:10.1016/j.jphotochem.2004.01.009

photoexcited TiO_2 to the surface adsorbed SCN^- in aqueous suspension. The observed rise components at 480 nm, with lifetimes less than 1 ps, few picoseconds and several hundreds picoseconds, were ascribed to the fast hole transfer, subsequent structure stabilization of the formed $(SCN)_2^{\bullet -}$, and slow hole transfer, respectively. The fast and slow hole transfers were considered to be due to surface trapped, or non-thermalized holes, and deeply trapped holes, respectively. Yang and Tamai [12] reported on a femtosecond study of charge carrier dynamics at TiO_2/SCN^- interface in colloidal solutions. The rate of the hole transfer from the TiO_2 colloid was reported to be comparable to that of the hole trapping, which was estimated to be less than 50 fs. The rise time of few picoseconds was ascribed to a formation of the weakly coupled dimeric radical anion, $(SCN\cdots SCN)^{\bullet -}$. The further structural change, resulting in the formation of stable $(SCN)_2^{\bullet -}$, was observed in a timescale of 100–150 ps. The proposed reaction scheme for the oxidation of SCN^- on TiO_2 surface was thus [12,18]:

$$h_{tr}^+ + SCN^- \rightarrow SCN^{\bullet} \quad (1)$$

$$SCN^{\bullet} + SCN^- \rightarrow (SCN\cdots SCN)^{\bullet -} \quad (2)$$

$$(SCN\cdots SCN)^{\bullet -} \rightarrow (SCN)_2^{\bullet -} \quad (3)$$

where h_{tr}^+ indicates the trapped hole.

The photocatalytic activity strongly depends on the physical properties of the TiO_2 particles e.g. crystal structures, particle sizes, surface areas, surface hydroxyls, defects, and impurities [3]. The charge carrier dynamics on the TiO_2 surface are influenced by these factors and thus it is crucial to study the ultrafast charge carrier dynamics of differently prepared TiO_2 photocatalysts particles. Only few reports, however, have been published concerning this subject [10,16,17].

The aim of the present work is to study the charge carrier dynamics of the TiO_2 particles calcinated at different temperatures in the presence and absence of SCN^- by means of the femtosecond diffuse reflectance spectroscopic measurements. The relation of the time-resolved spectroscopic results to the nature of the particles will be discussed. In addition, the kinetics of different steps of the SCN^- oxidation on the TiO_2 surface is described.

2. Experimental

2.1. Samples

Two series of TiO_2 nanocrystalline anatase powder samples calcinated at different temperatures, supplied by Kemira Pigments Oy (Pori, Finland), were examined. The physical properties of the samples are presented in Table 1.

2.2. Sample preparation

A sample preparation procedure, similar to that reported by Furube et al. [18], was used. Powder samples were added into the distilled water (100 g dm^{-3}). Suspensions were then diluted with water or 2 M KSCN water solution to final concentrations of 50 g dm^{-3} TiO_2 and 1 M KSCN. The pH of the suspensions were adjusted to a value of 1 by using the aqueous HCl solution. Samples were allowed to equilibrate overnight. For the time-resolved diffuse reflectance measurements, the samples were placed on a quartz cell (1 cm path length) and stirred with a magnetic stirrer to maintain uniformity throughout the experiment.

Table 1
The physical properties of the TiO_2 powder samples

Sample	Calcination temperature (°C)	Specific surface area ($m^2\ g^{-1}$)[a]	Primary particle size (nm)[b]
L81 300 °C	300	217	8
L81 450 °C	450	104	11
L81 550 °C	550	59	17
L81 650 °C	650	46	24
L135 300 °C	300	197	9
L135 450 °C	450	121	12
L135 550 °C	550	57	19
L135 650 °C	650	41	26

[a] Measured by the BET method (N_2 as adsorbate) using a Quantachrome Monosorb apparatus.
[b] Analysed by X-ray powder diffraction measurements.

2.3. Time-resolved diffuse reflectance spectroscopy

Femtosecond to picosecond time-resolved absorption spectra were measured using the pump-probe technique. The set-up is reported elsewhere [27]. Geometry of the detection part was modified for a diffuse reflectance mode. The femtosecond pulses of the Ti:sapphire laser were amplified by a multipass amplifier (CDP-Avesta, Moscow, Russia) pumped by a second harmonic of the Nd:YAG Q-switched laser (Solar TII, model LF114, Minsk, Belorussia). The amplified pulse energy varied from 0.4 to 0.5 mJ and the pulse repetition rate was 10 Hz. The second harmonic (400 nm) was used to excite the sample (pump beam). The remaining part of the light at main harmonic was focused into a quartz cell (0.5 cm path length) containing water to generate a white-light continuum (probe beam). The continuum was collimated by a lens and then split into two beams. The first beam was used as a probe beam for the transient diffuse reflectance measurements and it was focused on the same spot of the sample as the excitation beam. The second beam was used as a reference beam; it was focused on a non-excited area of the sample. The probe and the reference beams were collected by a lens and directed onto an input slit of a monochromator (Solar, Minsk, Belorussia) coupled with a cooled CCD detector (PI 1100 × 330, Princeton Instruments, USA). Each beam produced one stripe on the CCD image. The stripes were used to calculate intensity spectra for the signal, $I_{sig}(\lambda)$, and reference, $I_{ref}(\lambda)$, pulses. The wavelength range 460–680 nm was studied. The ratio of the intensities, $\alpha(\lambda) = I_{sig}(\lambda)/I_{ref}(\lambda)$, was typically within 0.8–1.3. The ratio was recorded before each measurement and was used

for the correction of the measured signals. For a single measurement, the CCD shutter was open for a period of 1 s and spectra of 10 pulses were averaged at once in the detector. Usually five measurements were performed and averaged to improve the signal-to-noise ratio. Intensities and shapes of the reference spectra were checked and variations of more than 10% were not accepted. Time-resolved spectra were measured with a delay line moving in 200 fs steps for the first 2 ps period and then increasing the time steps at longer delays. The whole time-range of interest (200 fs–1 ns) was measured with 40–60 spectra. Transient absorption intensity was displayed as percentage absorption given by:

$$\text{percentage absorption} = 100 \times \left(1 - \frac{R}{R_0}\right) \quad (4)$$

where R and R_0 represent intensities of the diffuse reflected white-light continuum with and without excitation, respectively. Time resolution of the system due to the diffuse reflectance method was not better than1 ps.

3. Results and discussion

3.1. Transient absorptions of TiO_2 suspensions

Transient absorption spectra of the TiO_2 powder samples in water suspensions were recorded at the wavelength range 460–680 nm. Multiexponential global fittings were applied to transient absorption decay curves at different wavelengths [27]:

$$D(t, \lambda) = a_0(\lambda) + \sum a_i(\lambda) \exp\left(\frac{-t}{\tau_i}\right) \quad (5)$$

where τ_i represent the lifetimes and $a_i(\lambda)$ the corresponding pre-exponential factors.

Three-exponential fittings gave reasonably good results for all the samples. The obtained transient absorption component spectra for the nanocrystalline anatase powder samples L81 and L135, calcinated at 300 and 650 °C, are shown in Fig. 1. The lifetime of the first component is on the lower limit of the time-resolution (about 1 ps) of the measurement system, and the lifetime of the third component is on the upper limit of the monitoring time-range (<1 ns). The normalized transient absorption decay curves for the sample L81, calcinated at 300, 450 and 650 °C, are shown in Fig. 2.

3.2. Character of photogenerated charge carriers

Broad transient absorptions covering the monitoring wavelength range 460–680 nm were observed in the absence of KSCN for all the samples (Fig. 1). The trapping of the conduction band electrons and the valence band holes at shallow or deep trapping sites is reported to occur in less than few hundred femtoseconds and the absorptions

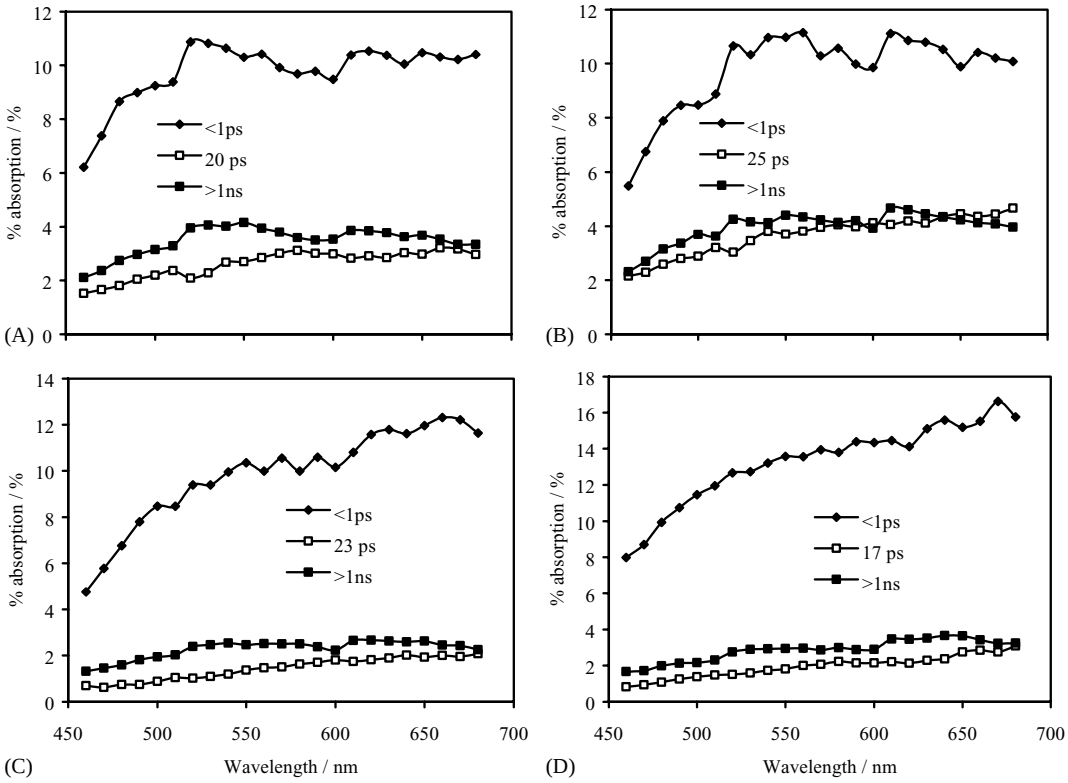

Fig. 1. Transient absorption component spectra of TiO_2 aqueous suspension (50 g dm^{-3}) at pH = 1: (A) L81 300 °C; (B) L81 650 °C; and (C) L135 300 °C; (D) L135 650 °C. (◆) First component, (□) second component, and (■) third component.

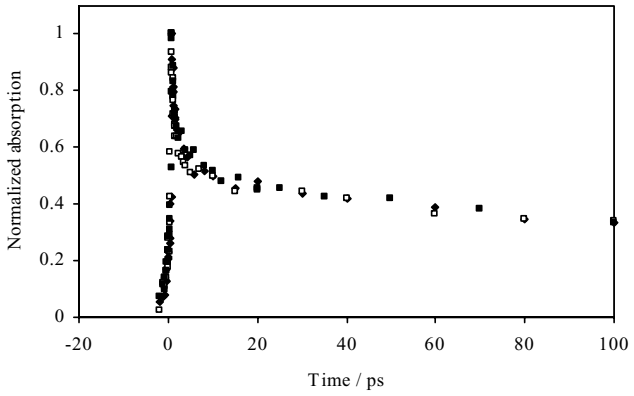

Fig. 2. Normalized transient absorption decay curves of TiO_2 aqueous suspension (50 g dm^{-3}) at pH = 1, monitoring wavelength 550 nm. (◆) L81 300 °C, (□) L81 450 °C, (■) L81 650 °C).

from the sub-picosecond to nanosecond timescales are ascribed to shallowly trapped and deeply trapped holes and/or electrons, respectively [9,11–13,17]. With regard to the previously published results, the first component is ascribed to the shallowly trapped holes and/or electrons and the following components are considered to arise from the electrons and/or holes trapped at different energetic states (e.g. deeply trapped holes and/or electrons).

3.3. Correlation of the transient absorption spectra and decay kinetics with the calcination temperature

Serpone et al. [10] reported that the decay times of the fast components decrease as the particle size increases. In addition, Ohtani et al. [16] reported that the calcination reduces the recombination rate of the electrons and holes. The reduced recombination rate was attributed to the reduced density of the surface crystal defects, which can act as recombination centers, and disappear with the increase in the calcination temperature.

In the present study, no essential differences were, however, observed in the decay dynamics of the particles calcinated at different temperatures. The shapes of the spectra, the relative amplitudes and the lifetimes of the components were about the same (Fig. 1). The similar decay kinetics is clearly seen in Fig. 2, where the normalized decay curves for the samples calcinated at different temperatures coincide.

3.4. Transient absorption measurements of TiO_2 suspensions in the presence of SCN^-

Transient absorptions of the TiO_2 powder samples in the presence of KSCN were measured in water suspensions at pH 1. Multiexponential global fittings were applied to the transient absorption decay curves at different wavelengths. Three-exponential fittings gave reasonably good results for all the samples. Transient absorption component spectra and the time-resolved spectra at different times of the nanocrystalline anatase powder sample L81, calcinated at 300, 450 and 650 °C, are shown in Fig. 3. The spectra were basically the same for the L135 series of samples (results not shown). The lifetimes of the first two components are summarized in Table 2 (the lifetime of the third component is longer than 1 ns for all the samples).

Table 2
The first and the second lifetimes for the measurements of the TiO_2 powder samples in water suspensions (50 g dm^{-3}) in the presence of KSCN (1 M) at pH 1

Sample	τ_1 (ps)	τ_2 (ps)
L81 300 °C	2.1	76
L81 450 °C	2.7	140
L81 550 °C	4.3	130
L81 650 °C	4.0	220
L135 300 °C	2.2	92
L135 450 °C	2.6	130
L135 550 °C	2.5	160
L135 650 °C	3.5	140

3.5. Mechanism and kinetics of the oxidation of SCN^- on the TiO_2 surface

At pH 1 the TiO_2 surface is positively charged and the SCN^- ions are adsorbed efficiently on its surface by electrostatic attractive forces. The association constant for the adsorption of SCN^- on the TiO_2 surface has been reported to be 350 M^{-1} in the acetonitrile solution [21]. Thus considering the experimental conditions, 50 g dm^{-3} TiO_2 and 1 M KSCN at pH 1, the adsorption sites should be almost fully occupied.

Transient absorption component spectra of the TiO_2 powder suspensions in the presence of SCN^- are shown in Fig. 3A, C and E. Because neither the adsorbed SCN^- ions nor the $SCN^\bullet$ radicals, formed after the hole transfer, do not absorb the light at the monitoring wavelength range the rate of the hole transfer could not be determined. The third component with the maximum around 500 nm and the lifetime much longer than the monitoring time-range (1 ns) evidently represents the spectrum of $(SCN)_2^{\bullet-}$. The spectrum is slightly shifted to the longer wavelength range as compared to the maximum value 480 nm reported in the literature [23]. The spectral shift is due to the absorption of the excited TiO_2 having an influence on the spectrum as some holes and electrons remain unrecombined at this timescale.

To discover the kinetics of the reaction, spectra of the intermediate states were calculated. As the lifetimes of the three components are not close to each other one can select delay times at which the transient absorption spectrum is dominated by one intermediate state. The spectrum of the first intermediate state of the sample is the spectrum immediately after the excitation and can be calculated using $t = 0$ ps in the Eq. (5). It represents the spectrum of the excited TiO_2, since the formation time of the second intermediate state is a few picoseconds and thus it cannot considerably affect the spectrum. The spectrum of the second

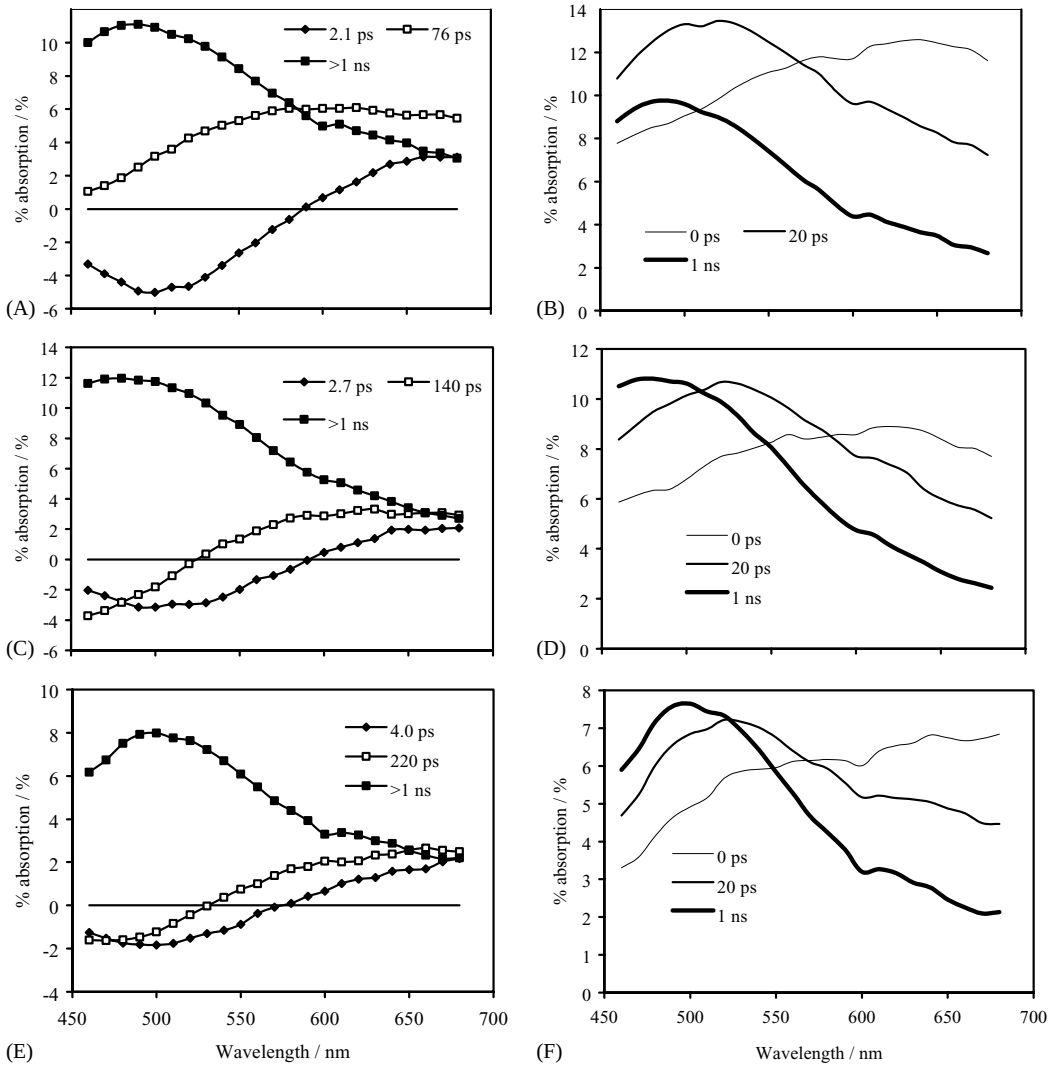

Fig. 3. Transient absorption component spectra of TiO_2 aqueous suspension (50 g dm^{-3}) in the presence of KSCN (1 M) at pH = 1 (A, C and E) and spectra at $t = 0$ ps, 20 ps and 1 ns (B, D and F): (A, B) L81 300 °C; (C, D) L81 450 °C; (E, F) L81 650 °C. (◆) First component, (□) second component, (■) third component.

intermediate state, formed with the time constant of a few picoseconds, can be obtained as time-resolved spectrum at $t = 20$ ps. At that delay time the second intermediate state is completely formed, but the following process, with a time constant of a few hundred picoseconds, have no effect on it. Correspondingly, the spectrum of the third intermediate state was calculated using $t = 1$ ns in the Eq. (5). At that time the first and the second intermediate states have totally decayed. The resulting spectra for the intermediate states of the L81 samples calculated from the corresponding component spectra (Fig. 3A, C and E) are shown in Fig. 3B, D and F. First of all, as already pointed out the spectrum at $t = 0$ ps represents the spectrum of the exited TiO_2. Secondly, the spectrum at $t = 1$ ns represent the spectrum of $(SCN)_2^{\bullet -}$ (with some contribution of the deeply trapped holes and/or electrons). The spectrum at $t = 20$ ps is shifted by 20 nm to the longer wavelengths as compared to the spectrum of $(SCN)_2^{\bullet -}$. Since deeply trapped holes and/or electrons (co-existing in time with SCN^- oxidation products) have broad spectra with the maximum at the red region (Fig. 1), the spectrum at $t = 20$ ps is attributed to the weakly coupled dimeric thiocyanate radical anion, $(SCN \cdots SCN)^{\bullet -}$. Its existence in reaction scheme has been proposed previously by Yang et al. [12] and Furube et al. [18]. Thus, the lifetimes of a few picoseconds correspond to the formation of $(SCN \cdots SCN)^{\bullet -}$. Then, the following structural stabilization yields $(SCN)_2^{\bullet -}$ in a few tens to hundreds of picoseconds depending on the calcination temperature. The possible reaction scheme for the oxidation of SCN^- on the TiO_2 surface is presented in Scheme 1.

3.6. The effect of the calcination temperature on the SCN^- oxidation

One effect of the increase in the calcination temperature is the decrease in the surface area. Thus the lower is the

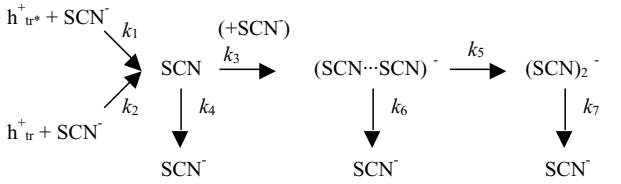

Scheme 1. Oxidation of SCN^- on the TiO_2 surface, h^+_{tr*} and h^+_{tr} represent shallowly and deeply trapped holes, respectively.

calcination temperature the higher is the amount of the adsorbed SCN^-. Thus the amount of the formed thiocyanate oxidation products can be expected to be higher. This is seen in the results as the negative value of a few picoseconds component at 500 nm increases with the decrease in calcination temperature (Fig. 3A, C and E), indicating that the amount of $(SCN\cdots SCN)^{\bullet -}$ formed in first few picoseconds is higher at low calcination temperatures.

The time constant of a few picoseconds and the time constant of a few hundred picoseconds increase when the calcination temperature is increased (Table 2). It is also observed for the samples calcinated at high and moderate temperatures, that the intensity of the absorption of $(SCN)_2^{\bullet -}$ at $t = 1$ ns relative to that of $(SCN\cdots SCN)^{\bullet -}$ at $t = 20$ ps is higher than for the samples calcinated at 300 °C (Fig. 3B, D and F). This indicates that the relative yield of the $(SCN)_2^{\bullet -}$ radicals increases with the increase in the calcination temperature.

The simplest interpretation for the faster formation times, when the calcination temperature is low, is that the rate constants of the formation of the $(SCN\cdots SCN)^{\bullet -}$ and $(SCN)_2^{\bullet -}$ states are higher (k_3 and k_5 in Scheme 1). The observable time constants are comprised, however, not only of the rates of the formation but also the rates of the other reaction steps e.g. disappearance of the reactants by other pathways. The observed time constant of a few picoseconds is a combination of at least two intrinsic rates: the formation of $(SCN\cdots SCN)^{\bullet -}$ (the rate constant k_3 in Scheme 1) and the relaxation of its precursor, $SCN^{\bullet}$, by, say, accepting e^- from TiO_2 particle (the rate constant k_4 in Scheme 1). If the relaxation rate of $SCN^{\bullet}$ does not interfere with the other rates, the first observed time constant is $\tau_1 = (k_3 + k_4)^{-1}$. Correspondingly, the time constant of a few hundred picoseconds is determined by the rate of the structural stabilization of $(SCN\cdots SCN)^{\bullet -}$ to form $(SCN)_2^{\bullet -}$ (the rate constant k_5 in Scheme 1), and the rate of its degradation to SCN^- (the rate constant k_6 in Scheme 1). As follows the faster formation times can indicate not necessarily the faster formation of the product, but also the faster relaxation of the reactant (by a side chain reaction) and as the result a less quantitative transformation of the precursors to the final oxidation products.

The increase in the relative amplitudes of $(SCN)_2^{\bullet -}$ compared to $(SCN\cdots SCN)^{\bullet -}$ with the increase in calcination temperature was observed. This also indicates the more quantitative transformation of $(SCN\cdots SCN)^{\bullet -}$ to $(SCN)_2^{\bullet -}$ for the particles calcinated at the higher temperatures, which can be well explained by the decrease of the side chain reaction (the rate constant k_6 in Scheme 1). Another factor which can contribute to this observation, and also to the longer time constants with the higher calcination temperatures, is the possible generation of new $(SCN)_2^{\bullet -}$ through reaction of SCN^- with the deeply trapped holes, still present after several picoseconds of excitation (the rate constant k_2 in Scheme 1). The data are not sufficient to substantiate involvement of the deeply trapped holes to the overall reaction.

With regard to the discussion above, the TiO_2 particles calcinated at the different temperatures show different reactivity to SCN^-. The amount of the fast hole transfer to SCN^- is higher for the particles calcinated at the low temperatures since the adsorbed amount of the SCN^- ions is higher. On the other hand, the relative amount of the $(SCN)_2^{\bullet -}$ formed during the time between few picoseconds to 1 ns compared to the amount of the initially formed $(SCN\cdots SCN)^{\bullet -}$ in few picoseconds is higher for the samples calcinated at the high temperatures. As discussed above this is caused by either the more quantitative transformation of $(SCN\cdots SCN)^{\bullet -}$ to $(SCN)_2^{\bullet -}$ or the slow hole transfer of the deeply trapped holes to SCN^-. This improvement is due to the change of the surface or bulk properties of TiO_2 caused by calcination e.g. increase in crystallinity and decrease of defects at high calcination temperatures.

4. Conclusion

The calcination of the TiO_2 particles at high temperatures increases the crystallinity, decreases the surface and bulk defects, and decreases the surface area of the particles. In the present study, the effect of the calcination temperature on the transient absorption properties of the TiO_2 particles has been examined.

The surface and bulk defects are generally considered to be as recombination centers for the photogenerated holes and electrons of the semiconductor particles. Thus the electron/hole recombination time was suspected to depend on the calcination temperature. In our study the calcination of the TiO_2 samples at different temperatures had, however, no effect on electron/hole decay dynamics.

The multiexponential global fitting analysis was applied to the transient absorption data of the TiO_2/SCN^- system. The resulting transient absorption component spectra revealed the spectra and the time constants of the two thiocyanate oxidation products: the weakly coupled dimeric thiocyanate radical anion $(SCN\cdots SCN)^{\bullet}$ and its rearrangement product, the stable $(SCN)_2^{\bullet -}$.

The intensities of the component spectra, corresponding to the formation of $(SCN\cdots SCN)^{\bullet -}$ and $(SCN)_2^{\bullet -}$, and the corresponding time constants depended on the calcination temperature. It was observed that the amount of the initial fast hole transfer from TiO_2 to SCN^- was higher

for the samples calcinated at the low temperatures, but the subsequent reactions leading to the final oxidation product $(SCN)_2^{\bullet -}$ were more quantitative for the particles calcinated at the high temperatures. It is also possible that, for the particles calcinated at the high temperatures, the deeply trapped holes are transferred to SCN^-. Thus the calcination affected the activity of the TiO_2 particles to oxidize SCN^- by many ways: the increased calcination temperature is beneficial in the sense that the defects of the particles are reduced. This is likely responsible for the more quantitative transformation of the initial SCN^- oxidation products to the final products and the possible slow hole transfer. The high calcination temperature is, however, detrimental in the sense that the surface area is reduced and thus the amount of the SCN^- ions capable to oxidative reaction is also low.

References

[1] P.V. Kamat, Chem. Rev. 93 (1993) 267–300.
[2] M.A. Fox, M.T. Dulay, Chem. Rev. 93 (1993) 341–357.
[3] D.F. Ollis, H. Al-Ekabi, Photocatalytic Purification and Treatment of Water and Air, Elsevier, Amsterdam, 1993.
[4] A. Hagfeldt, M. Grätzel, Chem. Rev. 95 (1995) 49–68.
[5] M.R. Hoffmann, S.T. Martin, W. Choi, D.W. Bahnemann, Chem. Rev. 95 (1995) 69–96.
[6] A.L. Linsebigler, G. Lu, J.T. Yates Jr., Chem. Rev. 95 (1995) 735–758.
[7] A. Mills, S. Le Hunte, J. Photochem. Photobiol. A 108 (1997) 1–35.
[8] A. Fujishima, T.N. Rao, D.A. Tryk, J. Photochem. Photobiol. C 1 (2000) 1–21.
[9] D.E. Skinner, D.P. Colombo Jr., J.J. Cavaleri, R.M. Bowman, J. Phys. Chem. 99 (1995) 7853–7856.
[10] N. Serpone, D. Lawless, R. Khairutdinov, E. Pelizzetti, J. Phys. Chem. 99 (1995) 16655–16661.
[11] D.P. Colombo Jr., K.A. Roussel, J. Saeh, D.E. Skinner, J.J. Cavaleri, R.M. Bowman, Chem. Phys. Lett. 232 (1995) 207–214.
[12] X. Yang, N. Tamai, Phys. Chem. Chem. Phys. 3 (2001) 3393–3398.
[13] D.P. Colombo Jr., R.M. Bowman, J. Phys. Chem. 99 (1995) 11752–11756.
[14] D.P. Colombo Jr., R.M. Bowman, J. Phys. Chem. 100 (1996) 18445–18449.
[15] T. Asahi, A. Furube, H. Masuhara, Chem. Phys. Lett. 275 (1997) 234–238.
[16] B. Ohtani, R.M. Bowman, D.P. Colombo Jr., H. Kominami, H. Noguchi, K. Uosaki, Chem. Lett. 7 (1998) 579–580.
[17] A. Furube, T. Asahi, H. Masuhara, H. Yamashita, M. Anpo, J. Phys. Chem. B 103 (1999) 3120–3127.
[18] A. Furube, T. Asahi, H. Masuhara, H. Yamashita, M. Anpo, Res. Chem. Intermed. 27 (2001) 177–187.
[19] A. Furube, T. Asahi, H. Masuhara, H. Yamashita, M. Anpo, Chem. Phys. Lett. 336 (2001) 424–430.
[20] S. Ikeda, N. Sugiyama, B. Pal, G. Maræi, L. Palmisano, H. Noguchi, K. Uosaki, B. Ohtani, Phys. Chem. Chem. Phys. 3 (2001) 267–273.
[21] P.V. Kamat, Langmuir 1 (1985) 608–611.
[22] J.H. Baxendale, D.A. Stott, Chem. Commun. 14 (1967) 699–700.
[23] L. Dogliotti, E. Hayon, J. Phys. Chem. 72 (1968) 1800–1807.
[24] R.B. Draper, M.A. Fox, J. Phys. Chem. 94 (1990) 4628–4634.
[25] D.W. Bahnemann, M. Hilgendorff, R. Memming, J. Phys. Chem. B. 101 (1997) 4265–4275.
[26] J.L. Ferry, M.A. Fox, Langmuir 14 (1998) 1725–1727.
[27] N.V. Tkachenko, L. Rantala, A.Y. Tauber, J. Helaja, P.H. Hynninen, H. Lemmetyinen, J. Am. Chem. Soc. 121 (1999) 9378–9387.